Results in Engineering 29 (2026) 109384

Contents lists available at ScienceDirect

Results in Engineering

journal homepage: www.sciencedirect.com/journal/results-in-engineering

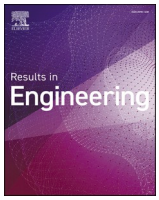

Research paper

A unified three-dimensional meshless analysis of vibration and thermal buckling of variable-thickness cylindrical shells

Reza Pilafkan [a,*], Vahid Arab Maleki [b]

[a] Department of Mechanical Engineering, University of Mohaghegh Ardabili, Ardabil, Iran
[b] Department of Mechanical Engineering, University of Maragheh, Maragheh, Iran

ARTICLE INFO

Keywords:
Cylindrical shell
Variable thickness
Three-dimensional elasticity
Meshless method
Thermal buckling

ABSTRACT

This paper presents a comprehensive analysis of free vibrations and thermal buckling of cylindrical shells with variable thickness, formulated based on three-dimensional elasticity theory and the variational principle. The governing equations are derived by considering geometric nonlinearities and uniform temperature distribution, then solved meshlessly using the Radial Point Interpolation Method (RPIM).The key innovation of this research lies in developing an accurate and integrated model that effectively simulates the complex effects of variable thickness on the dynamic behavior and thermal stability of shells under various boundary and thermal conditions. Numerical results demonstrate that thickness variations significantly influence natural frequencies and critical buckling loads, particularly under thermal loading and diverse boundary conditions, where the shell's behavior undergoes remarkable changes. A comparison with reference data confirms the accuracy and efficiency of the proposed model. This study provides valuable insights for the design and optimization of shell structures in thermal environments.

1. Introduction

The analysis of the dynamic behavior and thermal stability of cylindrical shells, especially when their thickness is variable, is a significant challenge in structural engineering [1–3]. These shells, due to their widespread applications in industries such as aerospace, energy, and marine structures, have always received considerable attention [4–6]. Variations in the thickness of these shells can have substantial effects on their vibrational properties and thermal stability, making accurate analysis crucial for optimizing the design and performance of complex structures [7–9]. Given the limitations of existing analytical models in predicting the behavior of shells with variable thickness, the use of advanced numerical methods, such as meshless techniques, in simulating the behavior of these shells under real-world conditions, especially under varying temperatures and complex loading scenarios, is of great importance.

In most studies, cylindrical shells have been analyzed using simplified theories since the use of three-dimensional elasticity theory leads to mathematical complexities in the governing equations [10–12]. While the accuracy of simplified theories is acceptable for thin shells, these theories lack sufficient accuracy for thick shells, requiring the use of higher-order theories [13–15]. Even for achieving acceptable precision, the use of three-dimensional elasticity theory is essential [16–18]. In the existing literature, various but limited theories have been proposed to explain the behavior of cylindrical shells with variable thickness. Wang et al [19] developed a dynamic model based on the precise transfer matrix method to investigate the vibrational behavior of cylindrical shells with variable thickness, observing this behavior by solving a set of first-order differential equations. Duan and Koh [20] presented analytical solutions for the transverse vibrations of cylindrical shells with uniformly varying thickness in arbitrary power-law forms, expressed in terms of generalized hypergeometric functions due to the forces acting in the transverse direction. Jiaet al [21] examined the free vibrations of stepped cylindrical shells with thickness variations in both the axial and circumferential directions based on Reissner's shell theory and a new symplectic mechanics approach. El-Kaabazi et al [22] studied the dynamic stiffness equations for cylindrical shells with variable thickness under the assumptions of Donnell, Timoshenko, and Flügge shell theories. For instance, Zhang et al [23] investigated vibration mitigation of doubly curved composite panels under transient dynamic loading by integrating advanced control schemes with optimization algorithms as well as machine learning techniques. Khoshgoftar et al [24] utilized

* Corresponding author.
E-mail address: rezapilafkan@uma.ac.ir (R. Pilafkan).

https://doi.org/10.1016/j.rineng.2026.109384
Received 29 November 2025; Received in revised form 1 January 2026; Accepted 30 January 2026
Available online 31 January 2026

second-order shear deformation theory as a higher-order shear deformation theory to analyze a functionally graded axisymmetric cylindrical shell with variable thickness.

A wide range of analytical, semi-analytical, and numerical methods have been developed and applied in the literature to investigate the vibration behavior of structural systems [25–27]. The finite element method is widely employed for vibration and thermal buckling analysis of shell structures by discretizing the three-dimensional elasticity equations into finite elements, enabling accurate modeling of complex geometries, boundary conditions, and thickness variations, and is commonly used as a benchmark for validating advanced numerical and meshless formulations [28,29]. Tang et al [17] presented a semi-analytical solution for analyzing the free vibrations of functionally graded cylindrical shells with variable thickness in two directions. In this model, the mechanical properties of the shells vary in both the axial and thickness directions. Sharafkhani et al [30] investigated the nonlinear mechanical behavior of circular functionally graded micro-plates subjected to combined electrostatic and mechanical shock loadings. Using a Galerkin-based reduced-order model and step-by-step linearization, they analyzed dynamic response, stability, and the influence of through-thickness material gradation on vibration characteristics. Alam et al [31] investigated the free vibrations of cylindrical shells in their study. The impact of various parametric ratios, such as the diameter-to-thickness ratio (D/t) and length-to-diameter ratio (L/D), on the vibrations of the shells was examined. These analyses were performed using the ANSYS Parametric Design Language (APDL) based on first-order shear deformation theory (FSDT) for different boundary conditions. Ameli-Basiri et al [32] analyzed the free vibrations of closed and open cylindrical shells using the state-space transformation concept, along with the Differential Transformation Method (DTM). The governing equations for these shells were developed based on Sanders' thin-shell theory and then transformed into a set of first-order differential equations, which were solved using the DTM method. Wang et al [33] developed a novel method for analyzing the free vibrations of moderately thick cylindrical shells. This method incorporates adaptive finite elements and crack damage simulation for analyzing natural frequencies. In this study, an iterative reverse method and error evaluation techniques, along with mesh refinement, were introduced to create a computational framework for vibration analysis of cracked cylindrical shells. Tong et al [34] proposed an analytical symplectic approach for studying the free vibrations of cylindrical shells. In this approach, symplectic space was used to systematically derive exact solutions without the need for trial functions. Taati et al [35] examined the free vibrations of cylindrical shells with variable thickness based on Donnell and Love's theories. They derived the governing equations and associated boundary conditions for these shells and presented a closed-form sixth-order frequency equation that investigates the effect of thickness variations on the natural frequencies and mode shapes of the shells. Grigorenko et al [36] analyzed the free vibrations of elliptical cylindrical shells with variable thickness using the modified Timoshenko-Mindlin theory. This study examined the effects of cross-sectional deformation, thickness variations, material properties, and boundary conditions on the natural frequency spectrum of the shells. Golpayegani et al [37] performed free vibration analysis of thin cylindrical shells made of functionally graded materials with linear thickness variations using finite element methods. The results of this study highlight the impact of thickness variations and boundary conditions on the natural frequencies of these shells. Kim et al [38] analyzed the vibrational behavior of cylindrical shells with variable thickness using the Haar wavelet discretization method. They developed theoretical formulations based on first-order shear deformation theory (FSDT) for these shells and calculated the natural frequencies and mode shapes. Grigorenko et al [39] also investigated the free vibrations of elliptical cross-sectional cylindrical shells with variable thickness using FEMAP software and the NASTRAN solver. These studies have taken significant steps in the analysis of vibrations and dynamic behavior of cylindrical shells with variable thickness. Each of these works, through the introduction of different methods and models, extensively contributes to the design and analysis of shell structures and paves the way for future research in this field [40–44].

There are various methods available for analyzing shells in this domain [45–47], but many of these methods face challenges such as the need for complex meshing, high computational complexity, and limited accuracy in modeling complex behaviors. In this context, meshless methods, such as the radial point interpolation method (RPIM), have been introduced as advanced tools for the precise and efficient analysis of cylindrical shells with variable thickness. These methods not only eliminate the need for meshing but also enable more accurate modeling of the structural behavior under non-uniform loading and temperature conditions. Li et al [48] presented a comprehensive numerical investigation of the free vibration behavior of rotating cross-ply laminated combined conical–cylindrical shells subjected to thermal environments. Their study employed a meshless Chebyshev-based RPIM within the framework of first-order shear deformation theory, accounting for centrifugal and Coriolis effects as well as thermal-induced nonlinear strain components. The reliability of their approach was demonstrated through extensive comparisons with established results, highlighting the effectiveness of meshless techniques for coupled shell systems under thermal and rotational effects. Liang et al [49] developed a novel three-dimensional vibration model for cylindrical shells based on full 3D elasticity theory using the Carrera unified formulation. By expanding displacement fields through Chebyshev polynomials and Taylor series and introducing artificial boundary surface springs, their model achieved high accuracy for arbitrary boundary conditions, as validated against finite element and literature results. More recently, other researchers have continued to extend advanced numerical frameworks—such as refined meshless schemes, unified formulations, and high-fidelity finite element models—to investigate the dynamic response of cylindrical and coupled shell structures under varying geometrical, boundary, and thermal conditions [50,51]. Li et al [52] developed a three-dimensional elasticity-based vibration model for cylindrical shells via the meshless method, enabling accurate prediction of dynamic behavior under general boundary conditions. Comprehensive reviews and recent advances in refined and three-dimensional shell theories were summarized by Mahmoud et al [53], highlighting the growing importance of 3D formulations for vibration and stability analysis. Despite these advances, most existing studies either focus on uniform-thickness shells or rely on conventional discretization strategies, indicating a clear need for robust three-dimensional and meshless formulations capable of simultaneously addressing thickness variation, boundary diversity, and thermal effects with verified accuracy.

The main innovation of this paper lies in the use of meshless methods for the three-dimensional free vibration analysis of thin and thick cylindrical shells with variable thickness under the influence of thermal buckling and temperature effects. While traditional methods face numerous limitations, this study significantly overcomes these constraints by employing the RPIM, offering a more flexible and accurate approach for modeling complex thickness variations and thermal conditions. This innovation has a significant impact on the precise prediction of natural frequencies and vibration behavior of cylindrical shells with variable thickness under complex thermal conditions, contributing greatly to the improved design and optimization of shell structures in various industries.

2. Radial point interpolation method (RPIM)

This section provides a concise overview of the RPIM. For more detailed explanations, refer to [38]. To interpolate a scalar field $\eta(\mathbf{x})$ in a three-dimensional domain V, N nodes are distributed at positions $\mathbf{x}_i (i = 1, 2, \ldots, N)$. In the meshless method, the value of $\eta(\mathbf{x})$ at any point $\mathbf{x}$ is approximated using function values from nodes within a local support domain around $\mathbf{x}$. Only these nearby nodes influence the interpolated

field at that point. This relationship can be expressed as follows:

$$\eta(x) = \sum_{i=1}^{n} \Phi_i(x)\widehat{\eta}_i = \Phi(x)\widehat{\eta} \tag{1}$$

where $\Phi_i(\mathbf{x})$ is the shape function at the i^{th} node that possess the Kronecker delta property and satisfy the partition of unity.

$$\Phi_i(\mathbf{x_j}) = \delta_{ij} \tag{2a}$$

$$\sum_{i=1}^{n} \Phi_i(x_j) = 1 \tag{2b}$$

To accurately capture stress gradients induced by axial thickness variation and three-dimensional deformation effects, a non-uniform nodal distribution is adopted in the present RPIM discretization. In the axial direction, the nodal coordinates are generated using a power-law stretching function as:

$$z_i = L\left(\frac{i}{N_z}\right)^{\beta}, \quad i = 0, 1, \ldots, N_z, \tag{3a}$$

where N_z denotes the number of nodes along the axial direction and β is a stretching parameter controlling the concentration of nodes. When β=1, a uniform nodal distribution is obtained, whereas β>1 results in increased nodal density in regions with higher thickness gradients.

For thick cylindrical shells, sufficient resolution through the thickness is ensured by adopting a non-uniform nodal distribution in the radial direction, given by:

$$r_j = r_{\text{in}} + h(z)\left(\frac{j}{N_r}\right)^{\gamma}, \quad j = 0, 1, \ldots, N_r, \tag{3b}$$

where N_r is the number of nodes in the radial (thickness) direction, r_{in} denotes the inner radius of the shell, and γ controls the clustering of nodes near the shell surfaces. Larger values of γ provide enhanced resolution in regions with high through-thickness stress gradients. The effectiveness of the adopted nodal distribution strategy is verified through the convergence studies reported in the Results section, which demonstrate that the computed vibration characteristics are insensitive to further nodal refinement.

The support domain is a subregion of the problem domain, centered at point **x**, that can have arbitrary shape and dimensionality. While spherical or cubic support domains are most commonly employed, other geometries are possible. The shape functions are constructed using radial basis functions (RBFs).

$$\eta(x) = \sum_{i=1}^{n} R_i(x)a_i + \sum_{j=1}^{m} P_j(x)b_j = R^T a + P^T b \tag{4}$$

In this formulation, R_i and P_i represent the n radial basis functions and m polynomial basis functions in the coordinates **x**, respectively, while a_i and b_i are unknown constants that will be derived later. To enhance accuracy and ensure interpolation stability, polynomial functions are incorporated into the model. The radial basis functions R_i depend on the distance s between the point **x** and a given node $\mathbf{x_i}$ within the support domain.

$$s = \sqrt{(x - x_i)^2 + (y - y_i)^2 + (z - z_i)^2} \tag{5}$$

Among various radial basis functions, the multi-quadric (MQ) function is adopted in this work due to its favorable properties.

$$R_i(\mathbf{x}) = \left(s^2 + (\alpha_c d_c)\right)^q \tag{6}$$

where α_c, d_c and q are shape parameters examined numerically. Meanwhile, the polynomial basis functions P_i provide completeness and improve conditioning of the system.

$$\mathbf{P}(\mathbf{x}) = \begin{bmatrix} 1 & x & y & z & x^2 & xy & xz & \ldots & P_m(\mathbf{x}) \end{bmatrix} \tag{7}$$

In the present RPIM formulation, the multi-quadric (MQ) radial basis function is employed, in which the shape parameters α_c, d_c and q play a crucial role in interpolation accuracy and numerical stability. Rather than performing a formal optimization, these parameters are selected based on a sensitivity-driven convergence and stability criterion, which is a common and effective practice in meshless methods.

Substituting Eq. (2) into (4) yields a system of equations that combines both radial basis and polynomial terms. This substitution ensures compatibility and enforces necessary constraints on the solution. The resulting system can be expressed in matrix form as:

$$\widehat{\eta} = \widehat{\mathbf{R}}\mathbf{a} + \widehat{\mathbf{P}}\mathbf{b} \tag{8}$$

where

$$\widehat{\mathbf{R}} = \begin{bmatrix} R_1(\mathbf{x_1}) & R_2(\mathbf{x_1}) & \ldots & R_n(\mathbf{x_1}) \\ R_1(\mathbf{x_2}) & R_2(\mathbf{x_2}) & \ldots & R_n(\mathbf{x_2}) \\ \ldots & \ldots & \ldots & \ldots \\ R_1(\mathbf{x_n}) & R_2(\mathbf{x_n}) & \ldots & R_n(\mathbf{x_n}) \end{bmatrix} \tag{9}$$

$$\widehat{\mathbf{P}} = \begin{bmatrix} 1 & x_1 & y_1 & P_m(\mathbf{x_1}) \\ 1 & x_2 & y_2 & P_m(\mathbf{x_2}) \\ \ldots & \ldots & \ldots & \ldots \\ 1 & x_n & y_n & P_m(\mathbf{x_n}) \end{bmatrix} \tag{10}$$

Considering Eq. (8), the system consists of n equations with $n + m$ unknowns. The required M additional equations are obtained by enforcing the polynomial reproduction constraints:

$$\widehat{\mathbf{P}}^T\mathbf{a} = 0 \tag{11}$$

Thus, by solving Eq. (8) using Eq. (11), we can express the variables **a** and **b** in terms of $\hat{\eta}$. These expressions can then be substituted into Eq. (4) to obtain a set of equations in the form of Eq. (1).

3. Governing equations

Consider an isotropic cylindrical shell with radius r, variable thickness $h(z)$ and length $L-L_0$, as depicted in Fig. 1. The thickness variation function is defined by $h(z)=h_0(z/L)^p$ that ho is the thickness at $z=L$ and p is the thickness variation parameter. The displacement field is defined in cylindrical coordinates, with displacements in the radial r, circumferential θ, and axial z directions:

$$\mathbf{u} = \begin{bmatrix} u & v & w \end{bmatrix}^T \tag{12}$$

where u, v, and w denote the displacements in the radial r, circumferential θ, and axial z directions, respectively.

The elastodynamic equation of homogeneous and isotropic cylindrical shell with density ρ is given by:

$$\mathbf{A}\sigma = \rho\ddot{\mathbf{u}} \tag{13}$$

where **σ** denotes the three-dimensional stress vector expressed in cylindrical coordinates, consisting of three normal stress components (σ_{rr}, $\sigma_{\theta\theta}$, σ_{zz}) and three shear stress components ($\sigma_{r\theta}$, σ_{rz}, $\sigma_{\theta z}$), and

$$\sigma = \begin{bmatrix} \sigma_{rr} & \sigma_{\theta\theta} & \sigma_{zz} & \sigma_{r\theta} & \sigma_{rz} & \sigma_{\theta z} \end{bmatrix}^T \tag{14a}$$

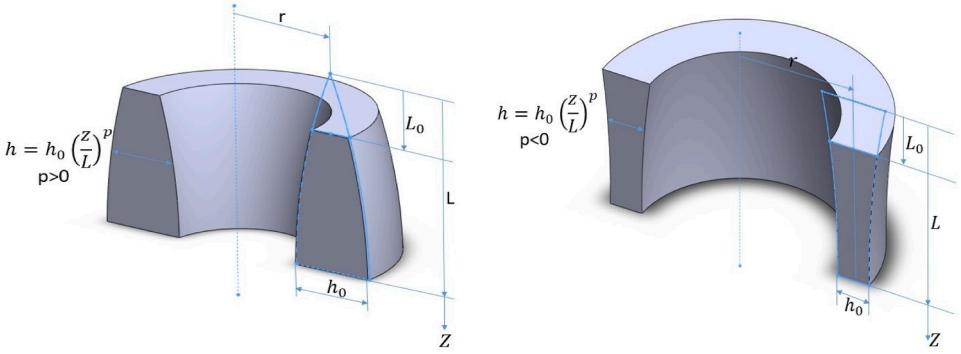

Fig. 1. Axial section of cylindrical shell with variable thickness.

$$\mathbf{A} = \begin{bmatrix} \frac{\partial}{\partial r} - \frac{1}{r} & -\frac{1}{r} & 0 & \frac{1}{r}\frac{\partial}{\partial \theta} & \frac{\partial}{\partial r} & 0 \\ 0 & \frac{1}{r}\frac{\partial}{\partial \theta} & 0 & \frac{\partial}{\partial r} + \frac{2}{r} & 0 & \frac{\partial}{\partial z} \\ 0 & 0 & \frac{\partial}{\partial z} & 0 & \frac{\partial}{\partial r} - \frac{1}{r} & \frac{1}{r}\frac{\partial}{\partial \theta} \end{bmatrix} \tag{14b}$$

The equation governing the relationship between stress and strain is given by:

$$\boldsymbol{\sigma} = \mathbf{D}\varepsilon \tag{15}$$

where

$$\boldsymbol{\varepsilon} = \boldsymbol{\varepsilon}_m - \boldsymbol{\varepsilon}_{th} \tag{16}$$

$$\boldsymbol{\varepsilon}_m = [\varepsilon_{rr} \quad \varepsilon_{\theta\theta} \quad \varepsilon_{zz} \quad \varepsilon_{r\theta} \quad \varepsilon_{rz} \quad \varepsilon_{\theta z}]^T \tag{17}$$

$$\boldsymbol{\varepsilon}_{th} = [\alpha_{rr} \quad \alpha_{\theta\theta} \quad \alpha_{zz} \quad \alpha_{r\theta} \quad \alpha_{rz} \quad \alpha_{\theta z}]^T = \alpha\Delta T \tag{18}$$

$$\alpha = [\alpha \quad \alpha \quad \alpha \quad 0 \quad 0 \quad 0]^T \tag{19}$$

where ΔT represents the temperature variation of the shell from the reference temperature to the buckling point, and α is the coefficient of thermal expansion and ε_m and ε_{th} is the mechanical and thermal strain respectively.

In this study, the temperature change ΔT is assumed to be uniform throughout the shell domain. Consequently, the thermal strain vector is spatially constant and expressed as $\varepsilon^{th}=\alpha\Delta T$, where α denotes the coefficient of thermal expansion. Under this assumption, thermal stresses are induced only through the mechanical constraints imposed by the boundary conditions, and no temperature gradient is considered in either the thickness or axial directions.

The equation that defines the relationship between strain and displacement fields is expressed as follows:

$$\boldsymbol{\varepsilon} = \mathbf{L}\mathbf{u} \tag{20}$$

The operator matrix is expressed as follows:

$$\mathbf{L} = \begin{bmatrix} \frac{\partial}{\partial r} & 0 & 0 \\ \frac{1}{r} & \frac{\partial}{r\partial \theta} & 0 \\ 0 & 0 & \frac{\partial}{\partial z} \\ 0 & \frac{\partial}{\partial z} & \frac{\partial}{r\partial \theta} \\ \frac{\partial}{\partial z} & 0 & \frac{\partial}{\partial r} \\ \frac{\partial}{r\partial \theta} & \frac{\partial}{\partial r} - \frac{1}{r} & 0 \end{bmatrix} \tag{21}$$

It is supposed that interpolation for a specific point in the shell is done using n nodes in the support domain of that point:

$$\mathbf{u} = \boldsymbol{\Phi}\hat{u} \tag{22a}$$

$$\hat{\mathbf{u}} = [u_1 \quad v_1 \quad w_1 \quad \ldots \quad u_n \quad v_n \quad w_n] \tag{22b}$$

Here, $\boldsymbol{\Phi}$ represents the shape function matrix of the RPIM. Substituting Eq. (22) into Eq. (20) results in:

$$\boldsymbol{\varepsilon} = \mathbf{L}\boldsymbol{\Phi}\hat{\mathbf{u}} - \alpha\Delta T = \mathbf{B}\hat{\mathbf{u}} - \alpha\Delta T \tag{23}$$

here, $\mathbf{B} = \mathbf{L}\boldsymbol{\Phi}$ represents the strain-displacement operator matrix. By substituting Eq. (23) into Eq. (17), we obtain:

$$\boldsymbol{\sigma} = \mathbf{D}\mathbf{B}\hat{\mathbf{u}} - \mathbf{D}\alpha\Delta T = \boldsymbol{\sigma}_{\mathbf{m}} - \boldsymbol{\sigma}_{\mathbf{th}} \tag{24}$$

The displacement fields for the cylindrical shell with variable wall thickness can be expressed as:

$$\begin{aligned} u(r,\theta,z,t) &= U(r,z)\cos(m\theta)e^{i\omega t} \\ v(r,\theta,z,t) &= V(r,z)\sin(m\theta)e^{i\omega t} \\ w(r,\theta,z,t) &= W(r,z)\cos(m\theta)e^{i\omega t} \end{aligned} \tag{25}$$

The circumferential dependence of the displacement components is expressed using orthogonal trigonometric functions, with u and w expanded in terms of $\cos(m\theta)$ and v in terms of $\sin(m\theta)$. This choice ensures periodicity and orthogonality of circumferential modes and

represents an equivalent modal description. The coupling between circumferential and torsional vibrations is inherently captured through three-dimensional strain components included in governing equations.

The displacement field formulation incorporates the circumferential mode number m and circular frequency ω, allowing different vibration modes m to be treated independently. For axisymmetric vibration $m = 0$, pure torsional modes can be obtained by interchanging the $\cos(k\theta)$ and $\sin(k\theta)$ functions in the modal representation. The displacement shape function matrix $\mathbf{\Phi}$ in Eq. (22) is derived from Eq. (1), where the nodal displacements $\hat{\mathbf{u}}$ follow the modal decomposition specified in Eq. (25). This formulation separates the spatial and temporal components of vibration, with $\mathbf{\Phi}$ capturing the spatial mode shapes while ω governs the harmonic time dependence:

$$[\mathbf{\Phi}] = \begin{bmatrix} \phi_1\cos(k\theta) & 0 & 0 & \dots & \phi_n\cos(k\theta) & 0 & 0 \\ 0 & \phi_1\sin(k\theta) & 0 & \dots & 0 & \phi_n\sin(k\theta) & 0 \\ 0 & 0 & \phi_1\cos(k\theta) & \dots & 0 & 0 & \phi_n\cos(k\theta) \end{bmatrix} \tag{26}$$

Note that the integration along the θ-direction is carried out analytically, as the shape functions are independent of θ.

After discretization using the meshless method and applying Hamilton's principle and the calculus of variations, the governing equations for free vibration and thermal buckling of cylindrical shells are obtained in the form of the following eigenvalue equations:

$$\mathbf{M}\ddot{\mathbf{u}} + (\mathbf{K} + \mathbf{K_{th}})\mathbf{u} = \mathbf{F} \tag{27}$$

where

$$M = \int_v \rho \Phi^T \Phi dV \tag{28}$$

$$K = \int_v B^{\mathrm{T}} \mathrm{DBdv} \tag{29}$$

$$K_{th} = \int_v \Phi^T \sigma_{th} \Phi dV \tag{30}$$

$$F = \int_v \Phi^T f_v dV - \int_A \Phi^T f_A dA \tag{31}$$

Consequently for free vibration and thermal buckling problems without body forces, the standard eigenvalue problem be solved as:

$$\left(\mathbf{K} - \omega^2 \mathbf{M}\right)(\mathbf{u}) = 0 \tag{32}$$

$$(\mathbf{K} - \lambda_{cr}\mathbf{K_{th}})(\mathbf{u}) = 0 \tag{33}$$

For convenience and comparison purposes, the critical thermal buckling temperature is expressed in terms of a nondimensional critical temperature parameter, defined as

$$\lambda_{cr} = \frac{\alpha E \Delta T_{cr}}{1 - \nu} \tag{34}$$

Here, ΔT_{cr} denotes the critical temperature increment corresponding to the onset of thermal buckling, at which the cylindrical shell loses its stability under uniform thermal loading. This parameter is adopted throughout the thermal buckling results to examine the effects of thickness variation, geometric ratios, and boundary conditions in a unified and dimensionless manner.

4. Results

This section presents and examines the results of free vibration and thermal buckling analyses for cylindrical shells with variable thickness, obtained using the RPIM. The effects of thickness variations on natural frequencies and critical buckling loads under different boundary conditions are first analyzed. Subsequently, the role of uniform temperature distributions in the thermal stability of the shells is evaluated. The obtained results are quantitatively and qualitatively compared with reference data, and the influences of geometric and thermal parameters on the dynamic and buckling behavior of the shells are discussed in detail. To account for the influence of boundary conditions on the free vibration and thermal buckling behavior of cylindrical shells, four distinct boundary conditions are considered: clamped (C), simply-supported Type-I (SS-SS Type-I), simply-supported Type-II (SS-SS Type-II), and free (F). The simply-supported boundary conditions are defined as follows:

$$u(r,\theta,z,t) = v(r,\theta,z,t) = 0 \;\; \sigma_{zz}(r,\theta,z,t) = 0 \;\; z = 0, L \tag{35a}$$

$$v(r,\theta,z,t) = w(r,\theta,z,t) = 0 \;\; \sigma_{rz}(r,\theta,z,t) = 0 \;\; z = 0, L \tag{35b}$$

The boundary conditions SS-SS Type-I and SS-SS Type-II correspond to two standard idealizations of simply supported cylindrical shells commonly adopted in the literature. While both configurations prevent rigid-body motion and allow free rotation, they differ in the imposed axial displacement and shear traction constraints. These definitions are consistent with classical shell vibration formulations and are introduced to examine the sensitivity of the dynamic response to boundary modeling assumptions.

4.1. Variable thickness thin cylindrical shell

A cylindrical shell with radius $r = 1$ m, L_0=0.8 m thickness $h_0 = 0.01$ m, and length L–L_0=0.2 m is analyzed. The material properties are specified as: Young's modulus E=70 GPa, Poisson's ratio ν=0.3, and mass density $\rho = 2700$ kg/m^3.

The frequency parameter ω_p defined as:

$$\omega_p = \frac{1}{\pi}\frac{12(1-\upsilon^2)}{(a/L)^2(h_0/L)^2}\left(\Omega^2(a/L)^2 - 1\right) \tag{36}$$

where the dimensionless frequency is $\Omega = \omega_p L\sqrt{\rho/E}$.

In the numerical simulations, the stretching parameters controlling the non-uniform nodal distribution are selected within the ranges β=1.2–1.8 for the axial direction and γ=1.5–1.7 for the radial (thickness) direction, which are found to provide stable convergence and sufficient resolution of thickness-induced stress gradients.

A series of numerical tests were conducted by varying d_c and q within

Table 1
Sensitivity of MQ–RPIM shape parameters on numerical accuracy and stability.

d_c	q	Conditioning of moment matrix	Change in first natural frequency
0.5	1.0	Poor (ill-conditioned)	Unstable / non-convergent
1.0	1.5	Moderate	< 1.2%
2.0	1.5	Well-conditioned	< 0.3%
3.0	2.0	Stable but over-smoothed	< 0.5%
5.0	2.0	Stable	< 1.0%

Table 2
Frequency parameter ω_p for thickness variation parameter $p = 1$ and C-C boundary condition.

N_r	N_z	ωp1	ωp2	ωp3	ωp4
17	46	7.138	11.6535	16.1233	20.4324
	47	7.138	11.6532	16.1228	20.4317
	48	7.138	11.6533	16.1233	20.4322
	49	7.138	11.6533	16.1234	20.4315
	50	7.137	11.6528	16.1224	20.4314
	51	7.137	11.6518	16.1212	20.4303
18	46	7.139	11.6546	16.1260	20.4384
	47	7.139	11.6542	16.1269	20.4395
	48	7.138	11.6542	16.1274	20.4373
	49	7.138	11.6538	16.1266	20.4364
	50	7.138	11.6542	16.1259	20.4373
	51	7.138	11.6541	16.1249	20.4386
19	46	7.139	11.6574	16.1298	20.4455
	47	7.139	11.6570	16.1291	20.4450
	48	7.139	11.6566	16.1298	20.4444
	49	7.139	11.6561	16.1293	20.4440
	50	7.139	11.6560	16.1288	20.4447
	51	7.137	11.6536	16.1248	20.4389
20	46	7.139	11.6560	16.1289	20.4443
	47	7.138	11.6559	16.1284	20.4437
	48	7.138	11.6556	16.1286	20.4433
	49	7.138	11.6553	16.1282	20.4431
	50	7.138	11.6547	16.1281	20.4435
	51	7.138	11.6548	16.1276	20.4431
21	46	7.139	11.6575	16.1319	20.4489
	47	7.139	11.6575	16.1317	20.4490
	48	7.139	11.6572	16.1314	20.4483
	49	7.139	11.6568	16.1309	20.4477
	50	7.139	11.6566	16.1305	20.4479
	51	7.139	11.6563	16.1309	20.4478

Table 3
Validation of the proposed RPIM formulation through comparison of frequency parameter ω_p for a thick cylindrical shell with linear varying thickness (p=1).

Method	Frequency parameter ω_p			
	First mode	Second mode	Third mode	Fourth mode
Ref [54]	7.1315	11.8397	16.5768	21.3127
FEM [54]	7.1386	11.6574	16.1354	20.4568
Proposed method	7.1389	11.6563	16.1309	20.4478
Difference with Ref [54] (%)	0.10	-1.57	-2.76	-4.23
Difference with FEM [54] (%)	0.00	-0.01	-0.03	-0.04

commonly accepted ranges to evaluate their influence on the conditioning of the moment matrix and on the computed natural frequencies. The objective was to identify a stable parameter region where the results become insensitive to further parameter variation while avoiding ill-conditioning. As summarized in Table 1, excessively small values of d_c lead to ill-conditioned interpolation matrices and numerical instability, whereas overly large values result in over-smoothed approximations with reduced accuracy. Within an intermediate stable region, the computed natural frequencies exhibit negligible sensitivity to changes in the MQ parameters. In particular, variations of d_c and q within this region result in changes of less than 0.3% in the first natural frequency, indicating a numerically converged and robust solution. Based on this observation, the parameter values highlighted in Table 1 were adopted in the present study to ensure a balanced compromise between accuracy and computational stability.

Table 2 reports the convergence behavior of the present RPIM discretization for a variable-thickness thin cylindrical shell with thickness variation parameter p=1 under clamped–clamped (C–C) boundary conditions. N_r and N_z denote the number of nodes in the radial r and axial z directions, respectively. The first four frequency parameters ω_{p1}–ω_{p4}, defined based on ω_p measure introduced in Eq. (36), are listed to assess numerical stability. The results exhibit negligible changes as N_r and N_z increase, indicating a well-converged solution and confirming that the adopted nodal discretization provides sufficient spatial resolution for accurate vibration prediction in the considered variable-thickness configuration.

Table 3 compares the frequency parameter ω_p of a thick cylindrical shell with linear varying thickness (p=1) obtained by the proposed RPIM-based formulation with the benchmark three-dimensional elasticity solutions reported by Duan and Koh [54] and the corresponding FEM results. For the first vibration mode, the difference between the present results and both reference and FEM solutions is negligible (below 0.1%), indicating excellent accuracy. As the mode order increases, slightly larger discrepancies are observed due to increased modal complexity; however, even in the worst case (fourth mode), the maximum deviation between the present results and the reference solution remains limited to approximately 4.23%, while the difference with FEM results does not exceed 0.04%. These results demonstrate that the proposed method achieves FEM-level accuracy and reliably reproduces benchmark solutions, thereby validating its suitability for dynamic and thermal stability analyses of cylindrical shells under various boundary and thermal conditions.

The fundamental frequency parameters for axisymmetric (m=0) and non- axisymmetric (m=1) vibration modes are presented in Figs. 2a and 2b, respectively, as functions of the thickness variation parameter for a

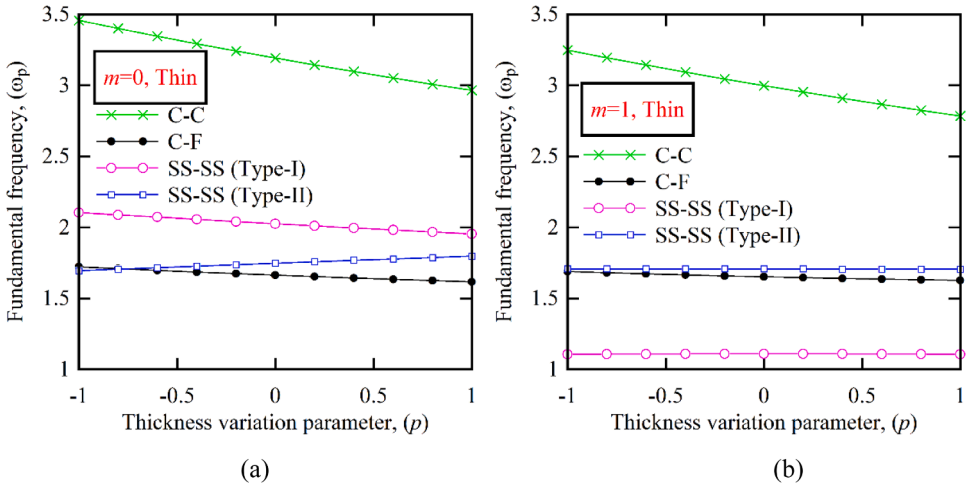

Fig. 2. Fundamental frequency (ω_p) of thin-walled cylindrical shell in terms of thickness variation parameter for different boundary conditions for (a) m=0, (b) m=1.

thin-walled cylindrical shell under different boundary conditions. The results indicate that under the clamped-clamped (C-C) boundary conditions, the natural frequency reaches its highest value, and as the thickness parameter increases from -1 to +1, the frequency decreases significantly. In the C-C case, the natural frequency decreases by approximately 20% when the thickness parameter changes from -1 to +1, whereas in the SS-SS Type-II case, the frequency variation is less than 5%. Under clamped-free (C-F) boundary conditions, a decreasing trend in frequency is also observed, but the extent is smaller. For simply supported Type-I (SS-SS Type-I) boundary conditions, the natural frequency is relatively lower and shows a slight increase as the thickness parameter rises. In contrast, under simply supported Type-II (SS-SS Type-II) conditions, the natural frequency remains nearly constant, with no significant change due to variations in thickness. These results demonstrate the significant influence of the variable thickness parameter and boundary condition type on the vibrational response of cylindrical shells, highlighting the importance of considering these factors in structural analyses. As seen in Fig. 2(b), in the non-axisymmetric (m=1) case under clamped-clamped (C-C) boundary conditions, the natural frequency exhibits a slight decrease with increasing thickness parameter, though this change is less pronounced compared to the axisymmetric case.

Under SS-SS boundary conditions particularly Type-II the natural frequency remains nearly constant, with thickness variation having little effect. These findings indicate that non-axisymmetric modes are less sensitive to thickness changes, and the vibrational behavior depends more strongly on boundary conditions. This further emphasizes the critical role of boundary condition and geometric parameters in the dynamic response of cylindrical shell structures.

Boundary conditions determine how much a shell can move or rotate at its edges; these constraints directly influence stress distribution, deformation, and vibrational behavior. When the shell's thickness varies, it's bending stiffness and mass distribution change across different sections. In C-C boundary conditions, the edges are highly restrained, so even slight changes in thickness distribution immediately translate into significant shifts in the system's overall stiffness and consequently, in its natural frequencies. However, under free or simply supported boundary conditions (especially Type-II, which allows greater freedom of movement), the edges permit more displacement and rotation. As a result, thickness variations have a weaker effect on the overall vibrational response. Simply put, the more constrained the boundary conditions, the more sensitive the system becomes to geometric changes (such as

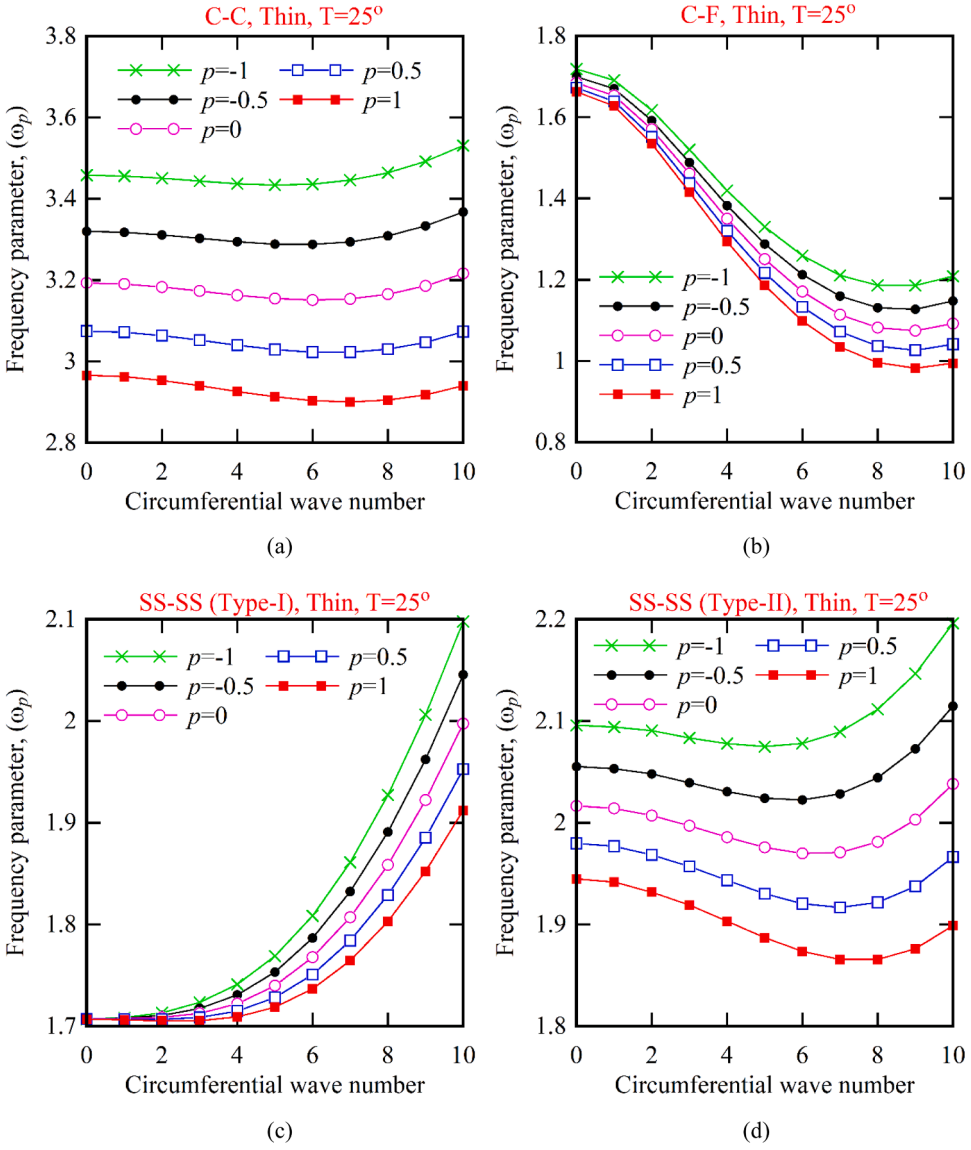

Fig. 3. Frequency parameter (ω_p) in terms of circumferential wave number of thin-walled cylindrical shell for (a) C-C (b) C-F (c) SS-SS Type-I (d) SS-SS Type-II boundary conditions.

Table 4
Frequency parameter ω_p under C−C boundary condition of thick cylindrical shell for $p = 0$.

N_r	N_z	m	$\Omega^{-}1$	m	$\Omega^{-}1$	m	$\Omega^{-}1$
10	18	0	1.572	1	1.312	2	1.594
	19		1.572		1.311		1.594
	20		1.572		1.311		1.593
	21		1.572		1.311		1.593
	22		1.571		1.310		1.593
	23		1.571		1.310		1.592
11	18		1.571		1.312		1.595
	19		1.571		1.311		1.594
	20		1.571		1.311		1.594
	21		1.571		1.311		1.593
	22		1.571		1.310		1.593
	23		1.571		1.310		1.593
12	18		1.571		1.312		1.595
	19		1.571		1.311		1.595
	20		1.571		1.311		1.594
	21		1.571		1.310		1.594
	22		1.571		1.310		1.594
	23		1.571		1.310		1.593
	Exact		1.571		1.308		1.594

variable thickness). Conversely, with freer or less restrictive boundaries, this sensitivity decreases, and the system's response depends more on edge mobility. Thus, the influence of shell thickness variations on vibrational behavior is directly linked to the degree of constraint or freedom in the boundary conditions. This explains why clamped shells show strong frequency shifts with thickness changes, while simply supported or free-boundary shells exhibit minimal variation.

Figs. 3a-3d illustrate the variation of the frequency parameter with respect to the circumferential wave number for different thickness variation parameters under C−C, C−F, SS−SS Type-I, and SS−SS Type-II boundary conditions, respectively. The results reveal that under clamped-clamped C−C boundary conditions, the frequency parameter exhibits significant variations when the thickness parameter is altered, regardless of the circumferential wave number. In contrast, for simply supported SS−SS Type-I and SS−SS Type-II boundaries, the frequency parameter remains relatively insensitive to thickness variations at low circumferential wave numbers, but the differences become more pronounced as the wave number increases. Interestingly, the clamped-free C−F boundary condition displays a distinct behavior, while the overall variation in the frequency parameter is substantial, the differences caused by thickness changes remain relatively small across all circumferential wave numbers. These findings highlight the strong influence of both thickness variation and boundary conditions on the vibrational response of thin cylindrical shells. Additionally, unlike cylindrical shells with uniform thickness, the lowest frequency in this study does not consistently correspond to the first non-axisymmetric mode ($m = 1$).

4.2. *Variable thickness thick cylindrical shell*

A thick cylindrical shell with radius $r = 1.5$ m, $h_0 = 0.1$ m, L=10 m and $L - L_0 = 4$ is analyzed. This study presents, for the first time, a three-dimensional investigation of natural frequencies for thick cylindrical shells with varying thickness under different boundary conditions. To validate the results, the frequency parameter ω_p is used, where r_o represents the outer radius at z=L. For negative values of the thickness variation parameter p, the shell thickness decreases toward one axial end. To preserve geometric admissibility and physical relevance, the minimum value of p is restricted to −0.4. For smaller values, the local thickness becomes excessively small, leading to unrealistic shell geometry and violating the applicability conditions of thick-shell modeling, although the thickness remains mathematically positive. Therefore, the chosen lower bound ensures a physically meaningful thickness distribution and numerical robustness.

Table 4 summarizes the effect of axial thickness variation on the frequency parameter ω_p of the cylindrical shell under the C-C boundary conditions. The results clearly demonstrate that the thickness gradient parameter significantly influences the dynamic response, with increasing thickness leading to higher stiffness and consequently higher natural frequencies. This highlights the importance of considering variable thickness distributions in realistic shell vibration analyses.

In Figs. 4 and 5, the effect of the thickness variation parameter and boundary conditions on the frequency parameter ω_p at 25°C is shown. In the thick-walled cylindrical shell, the minimum value of the thickness

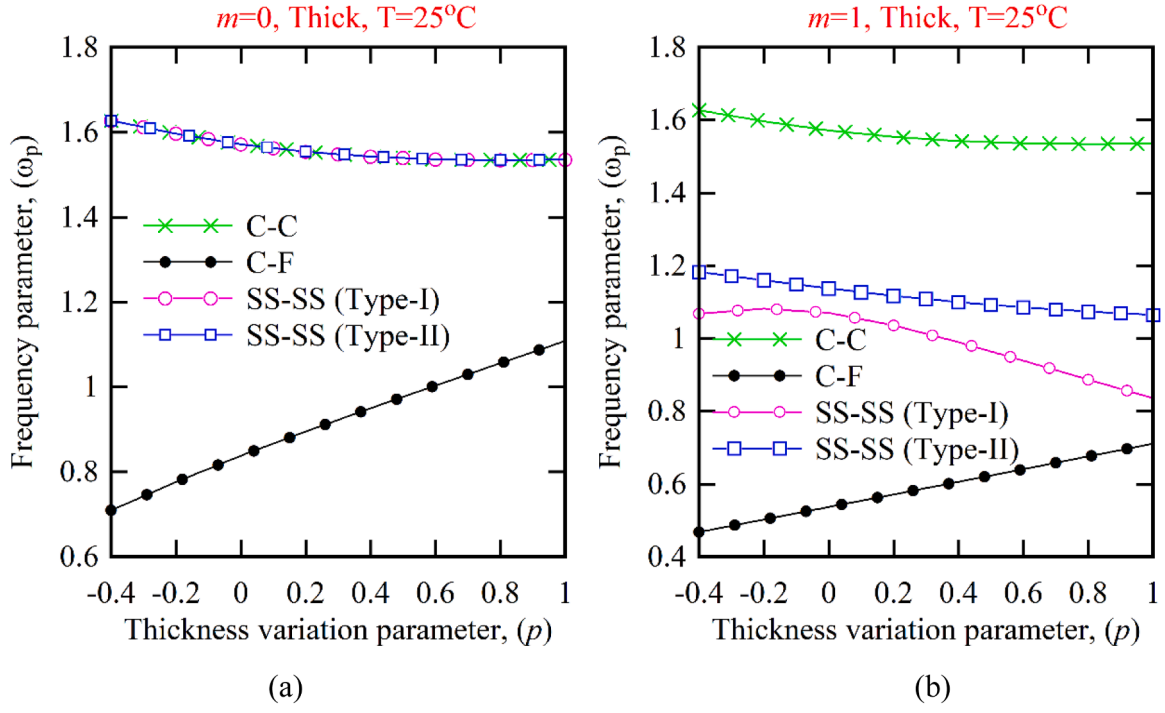

Fig. 4. Frequency parameter (ω_p) of thick-walled cylindrical shell in terms of thickness variation parameter for different boundary conditions for (a) m=0, (b) m=1.

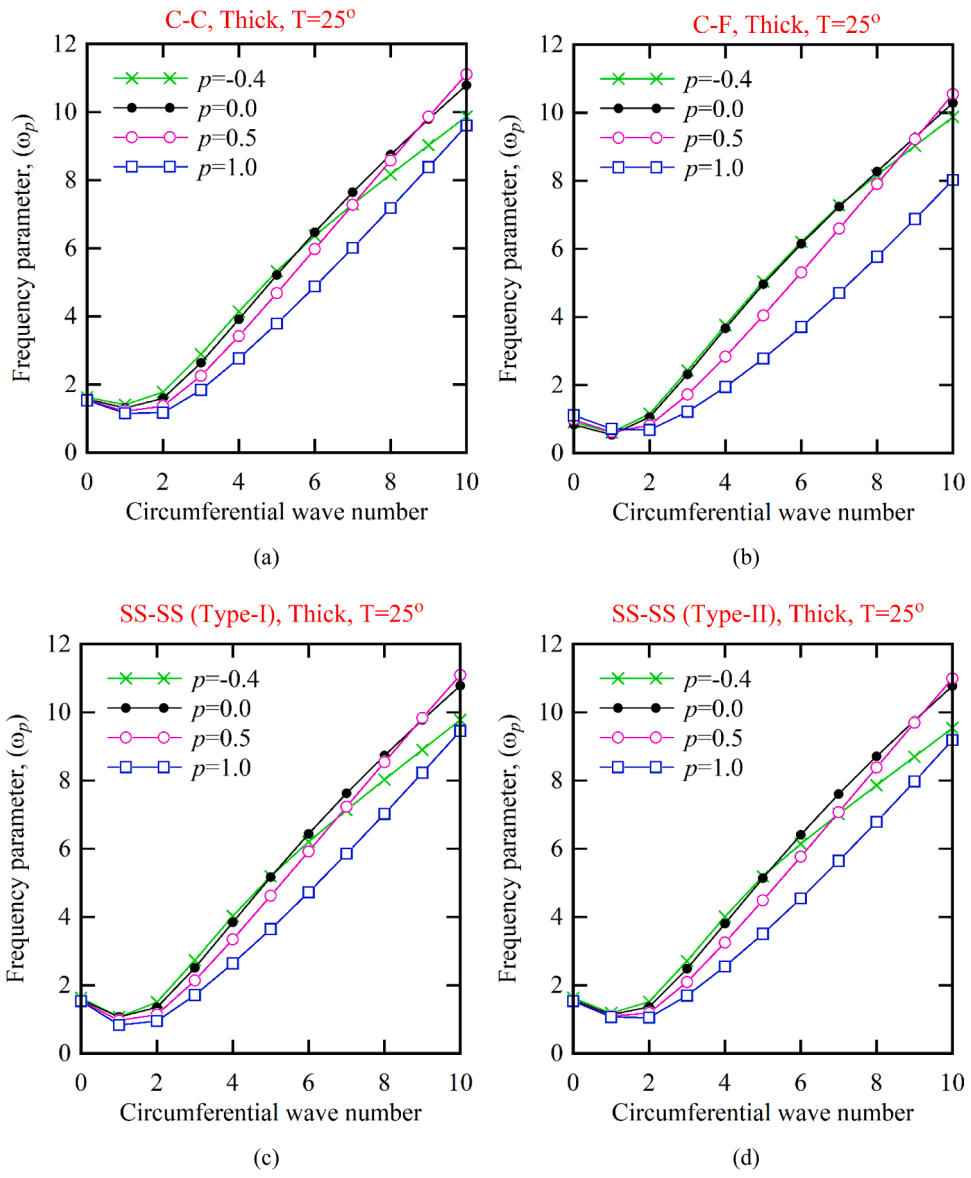

Fig. 5. Frequency parameter (ω_p) in terms of circumferential wave number of thick-walled cylindrical shell for (a) C-C, (b) C-F, (c) SS-SS Type-I, (d) SS-SS Type-II boundary conditions.

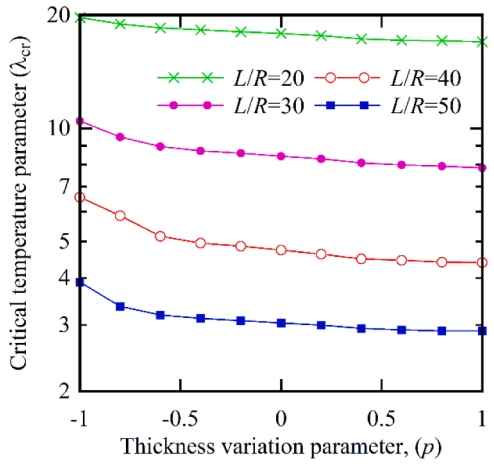

Fig. 6. The effect of length-to-radius ratio (L/R) on the critical temperature parameter of variable-thickness cylinders.

variation parameter (p) is set to -0.4 due to geometric constraints. From Fig. 4, which displays axisymmetric vibrations (m=0), it can be observed that the frequency variation in the C-C, SS-SS Type-I, and SS-SS Type-II boundary conditions is quite similar these boundary conditions have no effect on the frequency and show a clear difference compared to the C-F boundary condition. Additionally, the influence of the thickness variation parameter under these boundary conditions is similar but differs from the C-F case. It is clearly seen that the thickness variation parameter in the C-F case has a stronger effect on the frequency compared to other boundary conditions.

The natural frequency of vibrations under C-C, SS-SS Type-I, and SS-SS Type-II boundary conditions remains nearly constant and independent of the boundary conditions due to their strict constraints and edge fixity. These boundary conditions impose strong restrictions on edge displacements and rotations, stabilizing the distribution of vibrational mode shapes in such a way that thickness variations cannot induce significant changes in the overall structural stiffness. In fact, rigid boundary constraints tightly control the shell's vibrational behavior, homogenizing the effects of thickness variation across the structure. As a result, localized thickness changes in axisymmetric modes which exhibit

uniform vibration patterns have minimal impact on the natural frequency. Thus, under these conditions, natural frequencies depend more on local geometric variations (such as variable thickness) rather than on boundary conditions or edge constraints. Moreover, when boundary conditions are similar or closely related, their influence on natural frequency becomes negligible, making the frequency appear independent of boundary conditions. This phenomenon primarily occurs in axisymmetric modes and relatively uniform structures, where the vibration pattern is dominated more by geometric and material parameters than by edge constraints.

On the other hand, a comparison between Fig. 4a and Fig. 2 reveals that as the thickness changes from thin to thick, the trend of frequency variation remains similar under C-C and SS-SS Type-I boundary conditions but differs significantly under C-F and SS-SS Type-II conditions. This suggests that frequency variations depend more on thickness than on boundary conditions. However, these results do not hold for non-axisymmetric vibrations (m=1), as illustrated in Fig. 4b. For all boundary conditions except C-F, the natural frequency of non-axisymmetric vibrations decreases as the thickness variation parameter increases. Additionally, it is evident that SS-SS Type-I and C-F boundary conditions are more sensitive to thickness variations than the other two boundary conditions.

4.3. Thermal effects

Fig. 6 illustrates the influence of the length-to-radius ratio L/R of cylinders with variable thickness on the critical temperature parameter λ_{cr}. The results indicate that as the L/R ratio increases, the critical temperature parameter decreases significantly, demonstrating that longer cylinders exhibit reduced thermal buckling resistance compared to shorter ones. Additionally, variations in the thickness parameter p from negative to positive values lead to a gradual decrease in λ_{cr}, highlighting the detrimental effect of localized thickness increases on thermal stability. The highest λ_{cr} value corresponds to $L/R = 20$, while the lowest occurs at $L/R = 50$, confirming that shorter cylinders possess superior thermal resistance compared to longer ones. These findings underscore the critical role of geometric parameters and thickness variations in the design of cylinders under thermal loading, necessitating careful consideration in engineering analyses. As seen in Fig. 6, increasing the thickness parameter p, which corresponds to localized thickening, causes a gradual reduction in the critical temperature. However, this decline eventually stabilizes, with λ_{cr} converging to a constant value. This behavior suggests that beyond a certain thickness increase, further variations have a diminishing effect on thermal stability, and the system reaches a relatively steady state. Thus, excessive thickness modifications beyond this threshold do not significantly alter the critical temperature, indicating that the influence of parameter p is bounded.

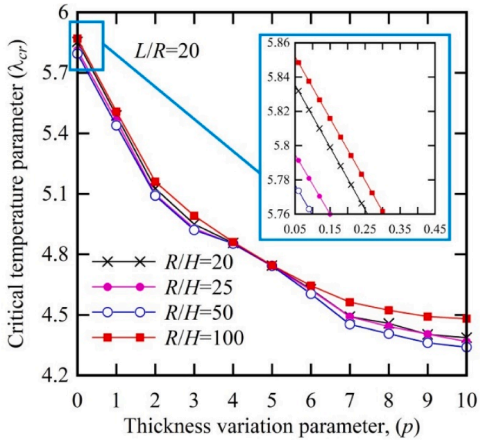

Fig. 7. The effect of the variable thickness radius-to-thickness ratio (R/H) on the critical temperature parameter.

Fig. 7 illustrates the effect of the radius-to-thickness ratio R/H in cylindrical shells with variable thickness on the critical temperature parameter. In this figure, four different cases of the radius-to-thickness ratio (R/H = 20, 25, 50, 100) are examined for a fixed length-to-radius ratio L/R = 20. As observed, as the thickness variation parameter p increases, indicating greater thickness inhomogeneity, the value of the critical temperature parameter decreases. This reduction demonstrates that thickness variation leads to a decrease in the thermal stability of the shell.

Additionally, as the radius-to-thickness ratio R/H increases, meaning thinner shells, the critical temperature parameter generally decreases, indicating that thinner shells are more sensitive to thermal effects. In the magnified section of the graph, the trend of the critical temperature parameter decreasing at low values of the thickness variation parameter p is displayed with greater precision, confirming a continuous and noticeable decline in this parameter even with slight increases in thickness variation. The parameter p represents the intensity of thickness variation along the shell. When p is small, the thickness is nearly uniform or exhibits minor variations, so the shell's thermal behavior is less sensitive to the radius-to-thickness ratio R/H. However, as p increases, thickness inhomogeneity becomes more pronounced, causing certain sections of the shell to become thicker or thinner.

This inhomogeneity leads to a non-uniform distribution of stiffness and mass in the shell, amplifying the effect of R/H. Shells with a large radius-to-thickness ratio (thin shells) are more sensitive to thickness variations and stiffness inhomogeneity due to their higher flexibility. At higher values of p, where thickness varies significantly, this sensitivity increases, resulting in more pronounced changes in the critical temperature parameter. Thus, thin shells (high R/H) under substantial thickness variation (hig hp) exhibit greater thermal instability, as reflected in the sharper decline of the critical temperature parameter.

4.4. Limitations of the meshless RPIM framework

Despite the flexibility and accuracy of meshless methods for problems involving smooth geometries and continuously varying material or geometric properties, the present RPIM-based formulation exhibits several limitations when applied to highly complex shell structures. First, the accuracy of RPIM strongly depends on the appropriate

Table 5
Comparison between RPIM (Meshless Method) and FEM for shell structure analysis.

Aspect	RPIM (Meshless Method)	FEM (Finite Element Method)
Geometric discretization	Node-based, no mesh required	Element-based mesh required
Handling variable thickness	Highly flexible for smooth thickness variation	Requires remeshing or special elements
Accuracy for smooth shells	High accuracy with proper node distribution	High accuracy with refined mesh
Complex shell geometry (cut-outs, sharp corners)	Limited; requires special treatment	Strong capability and mature tools
Boundary condition enforcement	More challenging for complex boundaries	Well-established and straightforward
Large deformation and strong nonlinearity	Limited without additional formulation	Well-developed nonlinear formulations
Computational cost (large-scale problems)	Higher due to dense interpolation matrices	Generally more efficient for large models
Mesh distortion issues	Not applicable	May occur for large deformations
Implementation complexity	Higher for complex geometries	Lower due to commercial solvers
Typical application domain	Smooth shells, graded thickness, vibration/buckling	General-purpose structural analysis

selection of support domain size, radial basis function parameters, and node distribution. For shells with severe geometric irregularities, sharp curvature transitions, or localized thickness discontinuities, improper parameter selection may lead to reduced accuracy or numerical instability. Second, while the meshless framework avoids mesh distortion issues commonly encountered in finite element methods, the imposition of complex boundary conditions on intricate shell edges or multi-connected domains remains challenging. The enforcement of displacement and traction constraints in RPIM generally requires additional treatments, which may increase implementation complexity for shells with non-standard boundaries. Third, the current formulation is developed under the assumption of moderate deformation and linear elastic material behavior. Consequently, its direct applicability to shells experiencing extremely large deformations, severe geometric nonlinearities, material plasticity, or damage evolution is limited without further extension of the governing equations and numerical scheme.

Finally, compared to conventional finite element approaches, meshless methods may incur higher computational cost for large-scale problems due to the construction and inversion of dense interpolation matrices. This aspect may restrict their efficiency when analyzing very large or highly detailed shell models unless advanced numerical acceleration techniques are employed.

Therefore, while the present RPIM framework is well suited for three-dimensional vibration and thermal buckling analysis of cylindrical shells with smoothly varying thickness, caution should be exercised when extending it to shells with highly complex geometries, severe deformities, or strongly nonlinear material behavior. As summarized in Table 5, the meshless RPIM framework offers distinct advantages for shell structures with smooth geometry and continuously varying thickness, particularly by avoiding mesh distortion and remeshing difficulties. However, for shells with highly complex geometries, sharp discontinuities, or severe deformation patterns, conventional FEM remains more robust due to its mature boundary enforcement techniques and well-established nonlinear formulations. The present study therefore focuses on a class of cylindrical shells for which RPIM provides an efficient and accurate alternative, while acknowledging that FEM may be more suitable for more geometrically intricate shell configurations.

5. Conclusions

This study presents a unified three-dimensional meshless RPIM framework for the vibration and thermal buckling analysis of cylindrical shells applicable to both thin and thick regimes. By directly modeling the three-dimensional displacement field, the proposed approach provides a consistent formulation without the need for thickness-dependent shell theories. The accuracy of the method is validated through comparisons with a well-established three-dimensional elasticity-based benchmark solution and independent three-dimensional finite element results, which is particularly relevant given the limited availability of benchmark data for thick cylindrical shells.

The results demonstrate that the proposed method achieves high accuracy for thin shells and maintains robustness for thick shells through appropriate nodal refinement in the thickness direction. Parametric studies reveal that thickness variation significantly affects both vibration characteristics and thermal stability. In particular, the critical temperature increases with the thickness variation parameter p and reaches a saturation regime at approximately $p \approx 6$, beyond which further increases in p have negligible influence. While the absolute critical temperature depends on the geometric ratios L/R and R/H, the saturation threshold with respect to p remains nearly unchanged for the range of geometries considered.

The meshless nature of the proposed formulation offers enhanced flexibility for modeling variable thickness distributions and complex boundary conditions, making it a promising alternative for advanced shell dynamics and thermal stability analyses. The present study is limited to shells with smooth geometric variation and quasi-static uniform thermal loading; extensions to transient thermal effects, thermal cycling, and more complex geometries are identified as important directions for future research.

CRediT authorship contribution statement

Reza Pilafkan: Writing – original draft, Visualization, Validation, Supervision, Software, Methodology, Formal analysis, Data curation, Conceptualization. **Vahid Arab Maleki:** Writing – review & editing, Conceptualization.

Declaration of competing interest

The authors declare that they have no known competing financial interests or personal relationships that could have appeared to influence the work reported in this paper.

All authors have reviewed the manuscript and approved its submission to the journal.

Data availability

The data that has been used is confidential.

References

[1] K. Chai, J. Liu, J. Lou, S. Liu, Vibration characteristics of cylindrical shells with discontinuous connections based on the spectral element method, Int. J. Solids. Struct. 308 (2025) 113148.
[2] X. Liu, W. Sun, H. Liu, H. Ma, D. Du, H. Li, An investigation of vibration responses for bolted composite flanged-cylindrical shells considering material and joint nonlinearity, Thin-Walled Struct. 204 (2024) 112335.
[3] A.E. Musa, M.M. Al-Ainieh, M.A. Al-Osta, Buckling of circular cylindrical shells under external pressures-A critical review, J. Constr. Steel. Res. 228 (2025) 109439.
[4] J.F. Derakhshandeh, Impact of length ratio on vibration frequencies and localized stress in flexible cylindrical shells: A comprehensive fluid structure interaction analysis, Phys. Fluids 37 (1) (2025) 36–52.
[5] S. Khan, A. Kumar, Buckling behaviour for advance cylindrical shells (COPV) subjected to extreme pressure conditions: A comprehensive review, Polym. Compos. 46 (9) (2025) 7785–7818.
[6] A. Ali, H. Hasan, M. Almabrouk, On the vibration and stability investigations of orthotropic FGMs plate and cylindrical shell: A review, Anbar J. Eng. Sci. 15 (1) (2024) 54–68.
[7] S. Javed, K. Viswanathan, Z. Aziz, Free vibration analysis of composite cylindrical shells with non-uniform thickness walls, Steel Compos. Struct. 20 (5) (2016) 1087–1102.
[8] L. Zhang, Y. Xiang, Vibration of open cylindrical shells with stepped thickness variations, J. Eng. Mech. 132 (7) (2006) 780–784.
[9] J.-H. Kang, Three-dimensional vibration analysis of joined thick conical—Cylindrical shells of revolution with variable thickness, J. Sound. Vib. 331 (18) (2012) 4187–4198.
[10] G. Iarriccio, A. Zippo, F. Pellicano, M. Barbieri, Resonances and nonlinear vibrations of circular cylindrical shells, effects of thermal gradients, in: Proceedings of the Institution of Mechanical Engineers, Part C: Journal of Mechanical Engineering Science 235, 2021, pp. 4818–4832.
[11] R. Hu, W. Wang, C. Zhang, Effect of preloading on vibration and buckling responses of variable stiffness composite cylindrical shells, Eng. Struct. 287 (2023) 116193.
[12] B. Ganendra, A.R. Prabowo, T. Muttaqie, R. Adiputra, R. Ridwan, A. Fajri, Q. Thang Do, H. Carvalho, S.J. Baek, Thin-walled cylindrical shells in engineering designs and critical infrastructures: A systematic review based on the loading response, Curved Layer. Struct. 10 (1) (2023) 20220202.
[13] M.H. Samadzadeh, M. Arefi, A. Loghman, Static bending analysis of pressurized cylindrical shell made of graphene origami auxetic metamaterials based on higher-order shear deformation theory, Heliyon. 10 (16) (2024) e36319.
[14] S. Shayanfar, A. Mamandi, Dynamic analysis of a thick-walled cylindrical shell subjected to an internal moving pressure load and temperature effect based on higher order deformation theory, Iran. J. Sci. Technol. Trans. Mech. Eng. 48 (3) (2024) 1283–1300.
[15] L. Zhang, W. He, S. Zhu, C. Lai, Y. Tao, H. Zhu, M. Li, H. Fan, Hierarchical lattice stiffened cylindrical shell: design, high-order vibration theory and composite parameter identification, Compos. Struct. 328 (2024) 117725.
[16] R. Springhetti, G. Rossetto, D. Bigoni, Buckling of thin-walled cylinders from three dimensional nonlinear elasticity, J. Elast. 154 (1) (2023) 297–323.
[17] L. Tang, D. Zhou, Vibrations of arbitrary deep and thick polymeric nanocomposite cylindrical panels: introduction of a novel quasi-3D shell model, J. Vib. Control 2025 (2025) 10775463251327825.

[18] R. Bina, M.S. Tehrani, A. Ahmadi, A.G. Taki, R. Akbarian, Using 3D theory of elasticity for free vibration analysis of functionally graded laminated nanocomposite shells, 52, Steel and Composite Structures, 2024, p. 487.
[19] X. Wang, H. Lin, Y. Zhu, W. Wu, Vibro-acoustic modelling of immersed cylindrical shells with variable thickness, Int. J. Nav. Archit. Ocean Eng. 12 (2020) 343–353.
[20] W. Duan, C. Koh, Axisymmetric transverse vibrations of circular cylindrical shells with variable thickness, J. Sound. Vib. 317 (3-5) (2008) 1035–1041.
[21] J. Jia, A. Lai, J. Qu, J. Zhao, J. Sun, Z. Zhou, X. Xu, C. Lim, Effects of local thinning defects and stepped thickness for free vibration of cylindrical shells using a symplectic exact solution approach, Acta Astronaut. 178 (2021) 658–671.
[22] N. El-Kaabazi, D. Kennedy, Calculation of natural frequencies and vibration modes of variable thickness cylindrical shells using the Wittrick–Williams algorithm, Comput. Struct. 104 (2012) 4–12.
[23] Q. Zhang, S. Han, M.A. El-Meligy, M. Tlija, Active control vibrations of aircraft wings under dynamic loading: introducing PSO-GWO algorithm to predict dynamical information, Aerosp. Sci. Technol. 153 (2024) 109430.
[24] M. Khoshgoftar, Second order shear deformation theory for functionally graded axisymmetric thick shell with variable thickness under non-uniform pressure, Thin-Walled Struct. 144 (2019) 106286.
[25] L. Rongzhou, R. Shuangxing, H. Lei, L. Zhonggang, C. Yushu, A.S. Nasser, S. M. Mohamed, Nonlinear vibration and stability analysis of an aero-engine dual-rotor system subjected to high-frequency excitation, Chin. J. Aeronaut. 38 (7) (2025) 103551.
[26] L.A. Al-Haddad, A.A. Jaber, M.N. Hamzah, H. Kraiem, M.I. Al-Karkhi, A. Flah, Multiaxial vibration data for blade fault diagnosis in multirotor unmanned aerial vehicles, Sci. Data 12 (1) (2025) 1383.
[27] N.A. Saeed, Y. Ellabban, L. Hou, G. Moatimid, S. Zhong, F.Z. Duraihem, Nonlinear dynamics of a bio-inspired 2-DOF low-frequency X-shaped vibration isolator with m-to-n layers driven harmonically under simultaneous primary and 1: 1 internal resonances, Chaos Solit. Fractals 190 (2025) 115786.
[28] S. Sourani Yancheshmeh, A. Ebrahimpour, T. Deemyad, Optimizing chassis design for autonomous vehicles in challenging environments based on finite element analysis and genetic algorithm. ASME International Mechanical Engineering Congress and Exposition, American Society of Mechanical Engineers, 2024.
[29] A. Mokhtarian, S. Babadoust, S. Salahshour, Transverse vibrations and stability of viscoelastic axially moving Rayleigh beams under thermal fields: an analytical approach, Appl. Eng. Sci. 22 (2025) 100233.
[30] N. Sharafkhani, G. Rezazadeh, R. Shabani, Study of mechanical behavior of circular FGM micro-plates under nonlinear electrostatic and mechanical shock loadings, Acta Mech. 223 (3) (2012) 579–591.
[31] I. Alam, A. Jain, Vibration analysis of cylindrical shells using finite element method, Nano World J. 9 (S1) (2023) S539–S543.
[32] M. Ameli-Basiri, M. Tavakkolizadeh, A. Aftabi-Sani, Free vibration analysis of closed and open horizontal cylindrical shells utilizing coupled transfer function method and differential transform method, Mech. Adv. Mater. Struct. 32 (13) (2024) 1–22.
[33] Y. Wang, J. Hu, D. Kennedy, J. Wang, J. Wu, Adaptive mesh refinement for finite element analysis of the free vibration disturbance of cylindrical shells due to circumferential micro-crack damage, Eng. Comput. 39 (9) (2022) 3271–3295.
[34] Z.Z. Tong, Y.W. Ni, Z.H. Zhou, X.S. Xu, S.B. Zhu, X.Y. Miao, Exact solutions for free vibration of cylindrical shells by a symplectic approach, J. Vib. Eng. Technol. 6 (2018) 107–115.
[35] E. Taati, F. Fallah, M.T. Ahmadian, Closed-form solution for free vibration of variable-thickness cylindrical shells rotating with a constant angular velocity, Thin-Walled Struct. 166 (2021) 108062.
[36] A.Y. Grigorenko, T. Efimova, Y.A. Korotkikh, Free vibrations of nonthin elliptic cylindrical shells of variable thickness, Int. Appl. Mech. 53 (6) (2017) 668–679.
[37] I.F. Golpayegani, E.M. Arani, A.A. Foroughifar, Finite element vibration analysis of variable thickness thin cylindrical FGM shells under various boundary conditions, Mater. Perform. Charact. 8 (1) (2019) 491–502.
[38] J. Kim, K. Kim, K. Kim, K. Hong, C. Paek, Free vibration analysis of cross-ply laminated conical shell, cylindrical shell, and annular plate with variable thickness using the haar wavelet discretization method, Shock Vib. 2022 (1) (2022) 6399675.
[39] A.Y. Grigorenko, M.Y. Borysenko, O.V. Boychuk, L.Y. Vasil'eva, Free vibrations of an open non-circular cylindrical shell of variable thickness. Analysis of Shells, Plates, and Beams: A State of the Art Report, Springer, 2020, pp. 141–154.
[40] G. Gârleanu, I. Mahariq, S. Saeidlou, D. Dobrotă, M.R. Tajbakhsh, Nonlocal dual-phase-lag thermoelastic damping in in-plane vibrations of rotating rectangular cross-sectional nanorings according to nonlocal elasticity theory, Acta Mech. 236 (2025) 5145–5165.
[41] Y. Pekbey, F.K. Maleki, H. Yildiz, G.G. Hesar, The meshless element free Galerkin method for buckling analysis of simply supported laminate composite plates, Adv. Compos. Lett. 21 (6) (2012) 096369351202100602.
[42] K.B. Bozdogan, F.K. Maleki, Application of differential transformation method for free vibration analysis of wind turbine, Wind Struct. 32 (1) (2021) 11–17.
[43] M.E. Toygar, O. Sayman, U. Kemiklioğlu, H. Öztürk, Z. Kıral, F.K. Maleki, Vibration and buckling analysis of a curved sandwich composite beam with FEM, Res. Eng. Struct. Mater. 2 (2016) 49–59.
[44] M. Ghasemi, A. Javid, Permeability estimation using rock physics modeling and variational Bayes inversion, Pet. Sci. (2025) (In Press).
[45] D. Zheng, J. Du, Y. Liu, Vibration characteristics analysis of an elastically restrained cylindrical shell with arbitrary thickness variation, Thin-Walled Struct. 165 (2021) 107930.
[46] S. Meng, R. Zhong, Q. Wang, X. Shi, B. Qin, Vibration characteristic analysis of three-dimensional sandwich cylindrical shell based on the spectro-geometric method, Compos. Struct. 327 (2024) 117661.
[47] K.R. Sivadas, N. Ganesan, Asymmetric vibration analysis of thick composite circular cylindrical shells with variable thickness, Comput. Struct. 38 (5) (1991) 627–635.
[48] Z. Li, S. Hu, R. Zhong, B. Qin, X. Zhao, Meshless Chebyshev RPIM solution for free vibration of rotating cross-ply laminated combined cylindrical-conical shells in thermal environment, Materials 15 (17) (2022) 6177.
[49] Liang, W. and T. Liu, (2023) Three-dimensional vibration model of cylindrical shells via Carrera unified formulation. 16(9):3345.
[50] S. Kwak, K. Ri, J. Kim, C. Pang, A meshfree approach for free vibration and stationary stochastic response analyses of functionally graded eccentric sectorial and annular plates, J. Braz. Soc. Mech. Sci. Eng. 47 (8) (2025) 397.
[51] J. Kim, D. Kang, K. Hong, C. Choe, U. Ri, A meshfree legendre point interpolation method for dynamic analysis of laminated composite double cylindrical and conical shells with bulkheads in thermal environment, J. Vib. Eng. Technol. 12 (3) (2024) 3797–3822.
[52] Z. Li, Q. Wang, R. Zhong, B. Qin, W. Shao, Vibration and damping analyses of sandwich cylindrical and conical shells using meshfree method, Eur. Phys. J. Plus 139 (6) (2024) 1–20.
[53] Z. Al Mahmoud, B. Safaei, S. Sahmani, M. Asmael, M.A. Shahzad, Q. Zeeshan, Z. Qin, Implementation of different types of meshfree technique in computational solid mechanics: a comprehensive review across nano, micro, and macro scales, Arch. Comput. Methods Eng. 31 (2) (2024) 725–838.
[54] W.H. Duan, C.G. Koh, Axisymmetric transverse vibrations of circular cylindrical shells with variable thickness, J. Sound. Vib. 317 (3) (2008) 1035–1041.